Journal of Alloys and Compounds 850 (2021) 156670

Contents lists available at ScienceDirect

Journal of Alloys and Compounds

journal homepage: http://www.elsevier.com/locate/jalcom

Influence of Al^{3+} on glass-forming ability, structural and electrical properties of the $Na_{3.4}Sc_2Si_{0.4}P_{2.6}O_{12}$ superionic conductor

Jairo F. Ortiz-Mosquera [a], Adriana M. Nieto-Muñoz [a, *], Ana C.M. Rodrigues [b]

[a] Programa de Pós-graduação em Ciência e Engenharia de Materiais, Universidade Federal de São Carlos, CP 676, 13565-905, São Carlos, SP, Brazil
[b] Departamento de Engenharia de Materiais, Universidade Federal de São Carlos, CP 676, 13565-905, São Carlos, SP, Brazil

ARTICLE INFO

Article history:
Received 7 June 2020
Received in revised form
27 July 2020
Accepted 8 August 2020
Available online 13 August 2020

Keywords:
NASICON Structure
Glass-ceramic
Bottleneck
Ionic conductivity
Solid electrolyte

ABSTRACT

This work reports the microstructure, and structural and electrical properties of $Na_{3.4}Al_xSc_{2-x}Si_{0.4}P_{2.6}O_{12}$ ($0.0 \leq x \leq 1.7$) NASICON (Na^+ Super-Ionic Conductor) compounds obtained from the crystallization of a precursor glass. The addition of aluminum in the $Na_{3.4}Sc_2Si_{0.4}P_{2.6}O_{12}$ NASICON composition improves the glass-forming ability of the precursor glass, which is evaluated by thermal analysis. Moreover, the Al^{3+}/Sc^{3+} isovalent substitution allows us to change the lattice parameters of the NASICON structure, without varying the number of charge carriers (Na^+ ions) per unit formula. X-ray diffractograms reveal the formation of the $Na_3Sc_2(PO_4)_3$ NASICON-type phase after crystallization of the parent glasses. From the structural characterization, it is also noted that the inclusion of Al^{3+} in the NASICON structure causes a volume contraction, which in turn, increases the activation energy and decreases the ionic conductivity. Thus, we demonstrated that the substitution of Sc^{3+} ions in the $Na_3Sc_2(PO_4)_3$ NASICON-type structure by an ion of the same valence, but with a smaller atomic radius, decreases the ionic conductivity of the material.

1. Introduction

The first compounds of the NASICON type family ($NaM_2(PO_4)_3$; M = Ge, Ti, Zr) were discovered in 1968 by Hagman and Kierkegaard [1]. The authors carried out an exhaustive analysis of the NASICON crystalline structure by X-ray diffraction and described it as an arrangement of PO_4 tetrahedra, which are connected by the vertices to the ZrO_6 octahedra when M = Zr. This special arrangement allows the formation of three-dimensional channels with bottlenecks through which Na^+ ions can move within the structure. However, it took eight years for the high conductivities achieved by these materials to be recognized. In 1976, Goodenough et al. [2] performed aliovalent substitutions Si^{4+}/P^{5+} in the material discovered by Hagman, and thus developed the $Na_{1+x}Zr_2Si_xP_{3-x}O_{12}$ ($0.4 \leq x \leq 2.8$) NASICON series. The ionic conductivity exhibited by these materials is among the most significant conductivities achieved in sodium ion-conducting compounds. The highest total ionic conductivity was obtained in the sample with $x = 2.0$ (6.7×10^{-4} S cm^{-1} at 25 °C and 2.0×10^{-1} S cm^{-1} at 300 °C). This high ionic conductivity is attributed to the introduction of extra Na^+ ions and also to the cell expansion, which was promoted by the Si^{4+}/P^{5+} substitution [2,3]. Since then, NASICON materials have been recognized as promising candidates as solid electrolytes [4] and also as cathode and anode materials in solid-state batteries [5].

In 2015, Guin et al. [6] added silicon to the $Na_3Sc_2(PO_4)_3$ system and synthesized a new $Na_{3+x}Sc_2Si_xP_{3-x}O_{12}$ ($0.1 \leq x \leq 0.8$) NASICON series. The highest total ionic conductivity of this series was found for the $x = 0.4$ composition and reached values of 6.9×10^{-4} S cm^{-1} and 3.8×10^{-1} S cm^{-1} at 25 °C and 300 °C, respectively. Recently, Zinkevich et al. [7] synthesized the same NASICON series and calculated the bulk conductivity from diffusion data estimated by NMR spectroscopy and using the Nernst-Einstein equation. The authors reported that the maximum bulk conductivity value was exhibited for sample $x = 0.5$ (1.82×10^{-3} S cm^{-1} at 25 °C), which is very similar to that for the sample $x = 0.4$ (1.65×10^{-3} S cm^{-1} at 25 °C). It is worth mentioning that these conductivities reported by Zinkevich et al. [7] and Guin et al. [6], are comparable to those reported by Goodenough et al. [2], thus indicating that this new $Na_{3+x}Sc_2Si_xP_{3-x}O_{12}$ NASICON series is very promising for its application as a solid electrolyte.

In the studies performed by Guin et al. and Zinkevich et al., the $Na_{3+x}Sc_2Si_xP_{3-x}O_{12}$ series was synthesized by a solid-state reaction. This synthesis route is one of the most used methods to obtain

* Corresponding author.
E-mail address: adrianamunoz@gmail.com (A.M. Nieto-Muñoz).

https://doi.org/10.1016/j.jallcom.2020.156670
0925-8388/

lithium and sodium ion-conducting NASICON materials [2,6–11]. However, over the past several years, the number of NASICON compounds obtained via the glass-ceramic route has increased due to various advantages compared with conventional methods [12–17]. Lower temperatures for crystallization of the precursor glasses, reduction in porosity, as well as the possibility of controlling the final microstructure of the material are some of the advantages that stand out from the glass-ceramic process [18,19]. To obtain a glass-ceramics, a precursor glass first needs to be synthesized, which can be achieved by several methods (melt-quenching, splat cooling and sol-gel [13,20,21]), and then crystallize it in a controlled process by applying suitable heat treatments.

Taking into account the high ionic conductivity exhibited by the $Na_{3.4}Sc_2Si_{0.4}P_{2.6}O_{12}$ compound [6], for the first time we report the synthesis of $Na_{3.4}Al_xSc_{2-x}Si_{0.4}P_{2.6}O_{12}$ ($0.0 \leq x \leq 1.7$) materials from the crystallization of the Na_2O–Al_2O_3-Sc_2O_3–SiO_2–P_2O_5 precursor glass. Note that we have added aluminum oxide to the original composition to improve the glass-forming ability of the precursor glass and also to evaluate the effect of the Al^{3+}/Sc^{3+} substitution on the lattice parameters of the NASICON structure. As reported [20,22], Al_2O_3 oxide can improve the glass-forming ability of precursor glasses of NASICON compounds. Besides, it has a much lower price compared to that of Sc_2O_3, which would make the $Na_{3.4}Al_xSc_{2-x}Si_{0.4}P_{2.6}O_{12}$ series more attractive in terms of cost.

It is worth mentioning that several aliovalent substitutions have been evaluated in the NASICON materials [2,4–6,15,16,22,23] to analyze their effect on structural and electrical properties. In fact, these substitutions promote an excess of negative charge that is compensated by the increase in the carrier concentration, which usually favors the conductivity of ionic compounds. However, in the present study, the number of charge carriers per unit formula is constant since we performed an isovalent substitution (Al^{3+}/Sc^{3+}) in the $Na_{3.4}Al_xSc_{2-x}Si_{0.4}P_{2.6}O_{12}$ NASICON series. This allows us to perform an original analysis about the evolution of the ionic conductivity based only on the variations of the lattice parameters, which directly influence the bottleneck size through which the Na^+ ions move within the material. In addition, we investigated the microstructural changes promoted by adding aluminum to the glass-ceramics.

2. Experimental procedures

2.1. Glass and glass-ceramics synthesis

Precursor glasses of nominal composition listed in Table 1 were synthesized from analytical grade Na_2CO_3 (Vetec, 99.5%), Al_2O_3 (Aldrich, 99.9%), Sc_2O_3 (ABCR, 99.9%), SiO_2 (Zetasil, 99%) and $(NH_4)_2HPO_4$ (Aldrich, 98%) in 7 g batches. The powder mixtures were homogenized with alumina balls in a rotary mill jar for 2 h and then heated from room temperature to 700 °C (10 °C min^{-1} heating rate). At this temperature, the precursor materials were calcined for 1 h to remove water (H_2O), ammonia (NH_3), and carbon dioxide (CO_2) from the raw materials. The batches were melted in a platinum crucible for 30 min at 1550 °C for the composition without aluminum ($x = 0.0$) and at 1450 °C for $x \geq 1.0$ samples, and later poured between two steel plates. Thus, glassy plates of 2 mm thickness were obtained. To release the thermal stresses, the obtained glasses were annealed for 2 h at a temperature below their glass transition temperature ($T_g - 40$ °C), previously determined by Differential Scanning Calorimetry (DSC), and then slowly cooled to room temperature inside the furnace.

Glass-ceramics of $Na_{3.4}Al_xSc_{2-x}Si_{0.4}P_{2.6}O_{12}$ ($1.0 \leq x \leq 1.7$) composition were prepared by heating the precursor glasses at their crystallization temperature (T_x) for 3 h. The heat treatments were performed in a tubular electrical furnace in an air atmosphere with temperature accuracy of ±1 °C.

Table 1
Nominal composition (mol %), glass transition (T_g) and crystallization (T_x) temperatures, and T_x - T_g stability parameter of $Na_{3.4}Al_xSc_{2-x}Si_{0.4}P_{2.6}O_{12}$ precursor glasses.

x	Na_2O	Al_2O_3	Sc_2O_3	SiO_2	P_2O_5	T_g [K]	T_x [K]	T_x - T_g [K]
			[mol%]			[±2 K]	[±2 K]	
0.0[a]	38.6	0.0	22.7	9.1	29.5	–	–	–
1.0	38.6	11.4	11.4	9.1	29.5	– [b]	850	–
1.2	38.6	13.6	9.1	9.1	29.5	827	880	53
1.5	38.6	17.0	5.7	9.1	29.5	780	895	115
1.7	38.6	19.3	3.4	9.1	29.5	723	905	182
2.0	38.6	22.7	0.0	9.1	29.5	684	– [b]	–

[a] Devitrified glass.
[b] Not observed on DSC thermograms.

2.2. Glass and glass-ceramic characterization

Glass transition (T_g) and crystallization (T_x, the onset of the crystallization peak) temperatures of $Na_{3.4}Al_xSc_{2-x}Si_{0.4}P_{2.6}O_{12}$ parent glasses were determined by Differential Scanning Calorimetry using a DSC-Netzsch 404 instrument at a heating rate of 10 °C min^{-1} using a platinum crucible in air atmosphere. The DSC analyses were done in monolithic samples.

X-ray diffraction analysis was performed to check the amorphous nature of the precursor glasses and to identify the crystallized phases in the glass-ceramics after the heat treatments. The data were obtained at room temperature, applying CuKα radiation generated at 20 mA and 40 kV in a Rigaku Ultima IV X-ray diffractometer. The X-ray patterns were collected in the 2θ angle range from 10° to 80°, with a step size of 0.02° and 0.6 s counting time. The crystalline phases were indexed using the Crystallographica Search-Match software [24]. The lattice parameters were determined by the Rietveld method using the Topas-Academic software (version 6) [25] in combination with the Inorganic Crystal Structure Database (ICSD) [26].

The microstructure of glass-ceramics was examined by means of scanning electron microscopy (SEM) using a Phillips XL30 FEG microscope. The micrographs were obtained on the fractured surfaces of samples previously sputtered with gold, applying a current of 20 mA and a time deposition of 15 s.

The electrical behavior of $Na_{3.4}Al_xSc_{2-x}Si_{0.4}P_{2.6}O_{12}$ glass-ceramics was analyzed by impedance spectroscopy using a NOVOCONTROL, Alpha-A High-Performance Frequency Analyzer. Impedance measurements were performed at temperatures between 50 and 300 °C (accuracy of 0.1 °C) within the 10 MHz–100 mHz frequency range and voltage amplitude of 300 mV. Before electrical measurements, both surfaces of the crystallized samples (~2 mm thickness and ~10 mm^2 surface) were initially sanded with 500 grit sandpaper to standardize the thickness of the samples and ensure parallel surfaces. In addition to removing small imperfections, sanding the samples also improves the adhesion of sputtered gold to the sample surface. Posteriorly, both surfaces were sputtered with gold electrodes using QUORUM Q150R ES equipment (current of 20 mA and time deposition of 300 s).

3. Results and discussion

3.1. DSC analysis

DSC thermograms of $Na_{3.4}Al_xSc_{2-x}Si_{0.4}P_{2.6}O_{12}$ parent glasses (Fig. 1) shows an endothermic event associated with the glass transition temperature (T_g), except for the samples with $x = 0.0$ and

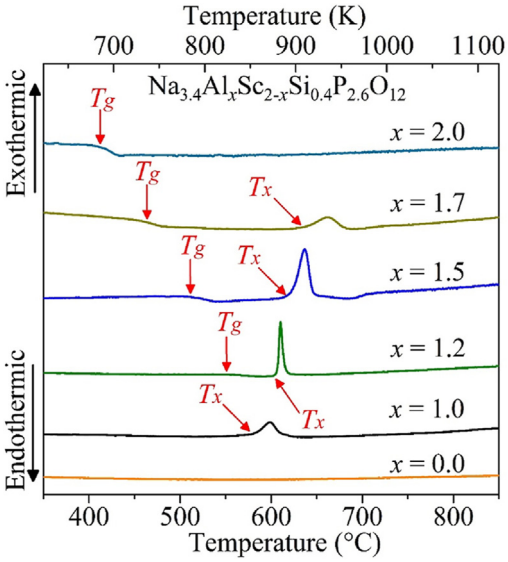

Fig. 1. DSC thermograms of $Na_{3.4}Al_xSc_{2-x}Si_{0.4}P_{2.6}O_{12}$ ($1.0 \leq x \leq 2.0$) parent glasses and of the devitrified sample ($x = 0.0$) obtained at a heating rate of 10 °C min^{-1} in air atmosphere. The positions of the glass transition (T_g) and crystallization (T_x) temperatures are indicated in the figure.

1.0. The absence of T_g and the crystallization peak (exothermic event) in the $x = 0.0$ composition is expected since this sample could not be vitrified. For this x value, the liquid crystallized completely during the cooling step of the synthesis. This spontaneous and uncontrolled crystallization process is known as devitrification. The devitrification of the $x = 0.0$ sample is probably due to the high percentage of Sc_2O_3 (see Table 1), which is not a glass-former oxide. Devitrified glasses are not considered as glass-ceramics (i.e., controlled crystallized glasses), and they may exhibit undesired properties mainly due to the non-uniform nature of their microstructure [27]. As mentioned in the introduction section, the improvement of the glass-forming ability of the $Na_{3.4}Sc_2Si_{0.4}P_{2.6}O_{12}$ original composition ($x = 0.0$) was one of the reasons for adding aluminum oxide in this series. In fact, it has been reported for other NASICON series that the aluminum oxide can improve the glass-forming ability of the precursor glass [20,22].

The glass-forming ability can be evaluated by the difference between the crystallization (T_x) and T_g temperatures, i.e., T_x - T_g [20,22,28]. The T_x - T_g glass stability parameter and the characteristic temperatures (T_g and T_x) of $Na_{3.4}Al_xSc_{2-x}Si_{0.4}P_{2.6}O_{12}$ parent glasses are summarized in Table 1. Since the T_x - T_g parameter increases with the increase of Al^{3+}, it is observed that the glass-forming ability and the thermal stability of glasses are improved by adding aluminum to the $Na_{3.4}Al_xSc_{2-x}Si_{0.4}P_{2.6}O_{12}$ ($1.2 \leq x \leq 1.7$) series. It is worth noting that a glass transition temperature (T_g) could not be detected for the $x = 1.0$ sample, which is attributed to the partial devitrification of the precursor glass. This assumption is corroborated by the low-intensity crystallization peak in the DSC (Fig. 1), and also by X-ray results, which will be shown in Fig. 2, section 3.2.

On the other hand, Fig. 1 also shows the absence of the crystallization temperature (T_x) in the $x = 2.0$ sample, which suggests high thermal stability against crystallization. In fact, the decrease in the intensity of the crystallization peak from the $x = 1.5$ to $x = 2.0$ samples, suggests that the presence of Al_2O_3 in the precursor glasses of the $Na_{3.4}Al_xSc_{2-x}Si_{0.4}P_{2.6}O_{12}$ series not only increases the glass stability parameter (T_x -T_g) but also hinders its crystallization. Similar behavior was reported in the precursor glasses of another silicon-containing NASICON series [15]. For this reason, the glass-ceramic with $x = 2.0$ was not analyzed.

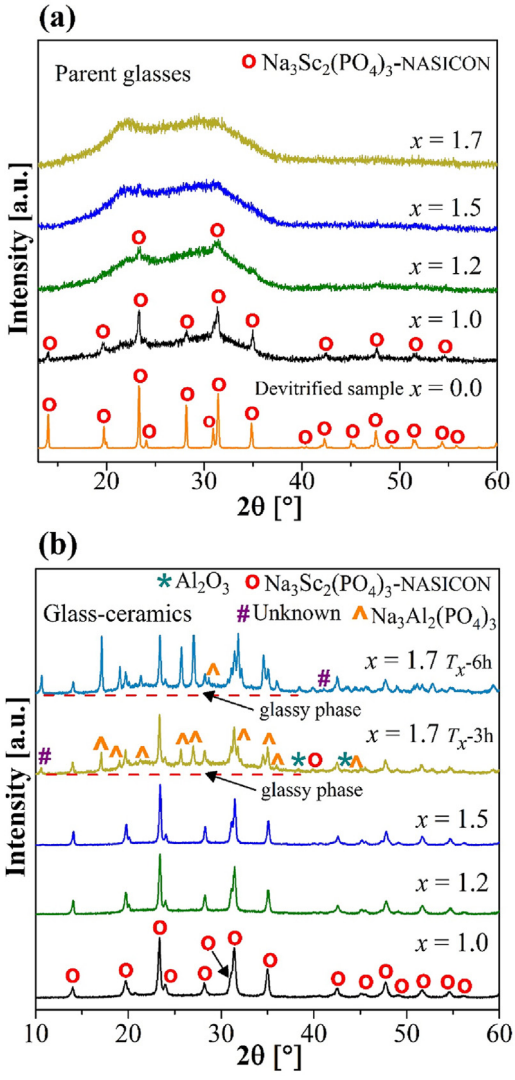

Fig. 2. (a) X-ray diffractograms of the $Na_{3.4}Al_xSc_{2-x}Si_{0.4}P_{2.6}O_{12}$ ($0.0 \leq x \leq 1.7$) as-prepared glasses and for (b) glass-ceramics ($1.0 \leq x \leq 1.7$) obtained with heat treatment at T_x for 3 h, and also for the $x = 1.7$ sample crystallized for 6 h.

3.2. X-ray diffraction

Fig. 2 presents the X-ray diffraction patterns of parent glasses and glass-ceramics of the $Na_{3.4}Al_xSc_{2-x}Si_{0.4}P_{2.6}O_{12}$ series. From Fig. 2a, it is noted that the $Na_{3.4}Sc_2Si_{0.4}P_{2.6}O_{12}$ sample (without aluminum, $x = 0.0$) presents intense diffraction peaks, which are associated with the $Na_3Sc_2(PO_4)_3$ NASICON-type (ICSD Filecard No. 239919). We remind here that this is a devitrified sample, i.e., the liquid crystallized during the cooling, as mentioned in section 3.1. The presence of some diffraction peaks of the $Na_3Sc_2(PO_4)_3$ NASICON phase can also be observed for the parent glasses with $0.0 < x \leq 1.2$ (Fig. 2a). However, it is noted that the intensity of these crystalline peaks decreases remarkably as the amount of aluminum increases. In fact, these diffraction peaks disappear in high-aluminum content samples ($x \geq 1.5$). Thus, these results demonstrate that the addition of aluminum oxide reduces the tendency to the devitrification, being highly useful to improve the glass-forming ability of the $Na_{3.4}Al_xSc_{2-x}Si_{0.4}P_{2.6}O_{12}$ compounds.

After crystallization heat treatments, the desired NASICON-type phase $Na_3Sc_2(PO_4)_3$ is present in all glass-ceramics (see Fig. 2b). However, this phase is observed as a single phase in glass-ceramics only for $1.0 \leq x \leq 1.5$ thus, suggesting that only the parent glasses with $x \leq 1.5$ are stoichiometric, i.e., they crystallize into a crystal with the same chemical composition [16]. Additionally, the $Na_3Al_2(PO_4)_3$ (JCPDS Filecard No. 31-1265) and Al_2O_3 (ICSD Filecard No. 064713) secondary phases appear for the glass-ceramic with the highest aluminum content ($x = 1.7$, Fig. 2b), inferring that the solid solution limit in $Na_{3.4}Al_xSc_{2-x}Si_{0.4}P_{2.6}O_{12}$ ($1.0 \leq x \leq 1.7$) series was reached at a value of $x = 1.5$. Thus, $x = 1.7$ sample crystallizes preferentially in the $Na_3Al_2(PO_4)_3$ phase, because of its high aluminum content. Some peaks of an unknown phase are also noticed in the $x = 1.7$ samples crystallized at T_x for 3 h and 6 h.

On the other hand, the presence of an amorphous halo between $20° < 2\theta < 30°$, characteristic of phosphate NASICON glasses [16,22] is also seen for the $x = 1.7$ glass-ceramics (Fig. 2b). This result reveals the presence of a residual glassy phase after the heat treatment performed at T_x (905 K) for 3 h and even in the sample treated for a longer time (see Fig. 2b). Thus, the total crystallization of this sample was not achieved at those thermal conditions. Besides, a high value of the glass stability parameter and a low-intensity crystallization peak has already been noticed in the thermal characterization of the $x = 1.7$ sample (section 3.1).

The data obtained by Rietveld analysis of the X-ray patterns of $Na_{3.4}Al_xSc_{2-x}Si_{0.4}P_{2.6}O_{12}$ ($1.0 \leq x \leq 1.5$) glass-ceramics, describing the crystallized NASICON structure are summarized in Table 2. Fig. 3 illustrates, as an example, the good agreement between the experimental and calculated patterns for the sample with $x = 1.0$. A similar result was obtained for other investigated samples. From Table 2, it is interesting to note a decrease in the unit cell volume of the NASICON structure as Al^{3+} is added. The contraction in the rhombohedral unit cell is caused by the decrease in the "*a*" lattice parameter. In fact, the incorporation of aluminum ions of smaller ionic radius (Al^{3+}: 0.535 Å) in the octahedral positions of scandium (Sc^{3+}: 0.745 Å) [29] is responsible for the contraction in the unit cell volume. As reported in several studies, the decrease in the cell volume also suggests a shrinkage of the bottleneck size of the NASICON structure due to the direct relationship between these two parameters [3,15,30].

The bulk crystal densities (ρ_{bc}) of $Na_{3.4}Al_xSc_{2-x}Si_{0.4}P_{2.6}O_{12}$ compounds (listed in Table 2) were calculated from the formula weight (F_w), the number of unit formula per NASICON unit cell ($Z = 6$, according to ICSD No. 239919), the calculated unit cell volumes (V) by Rietveld refinement and the Avogadro's number according to the expression [31]:

$$\rho_{bc} = F_w Z / N_A V \quad (1)$$

Table 2
Lattice parameters ($a = b$, c), unit cell volume (V) of rhombohedral $Na_3Sc_2(PO_4)_3$ NASICON structure, R_{wp} factor estimated by Rietveld analysis, formula weight (F_w) and bulk crystal densities (ρ_{bc}) for $Na_{3.4}Al_xSc_{2-x}Si_{0.4}P_{2.6}O_{12}$ glass-ceramics. The number within parentheses corresponds to the error in the last digit, given by the TOPAS software.

Sample	F_w	a	c	V	ρ_{bc}	R_{wp}[a]
x	[g.mol^{-1}]	[Å]	[Å]	[Å^3]	[g.cm^{-3}]	%
0.0	451.829	8.9400(3)	22.274(5)	1541.7(1)	2.920	10.53
1.0	433.855	8.880(1)	22.257(3)	1520.1(4)	2.845	8.57
1.2	430.260	8.869(9)	22.282(3)	1518.1(3)	2.825	8.04
1.5	424.868	8.865(1)	22.287(2)	1516.9(3)	2.792	8.86

[a] $R_{wp} = \Sigma [w(Y_{obs} - Y_{cal})^2 / \Sigma w Y_{obs}^2]^{1/2}$; Y_{obs} = Intensity of observed X-ray pattern, Y_{cal} = Intensity of calculated X-ray pattern, $w = 1/Y_{obs}$.

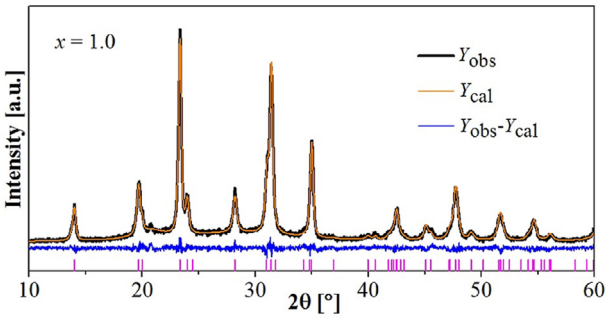

Fig. 3. Rietveld refinement of X-ray data of the $Na_{3.4}Al_xSc_{2-x}Si_{0.4}P_{2.6}O_{12}$ sample with $x = 1.0$. The Bragg peaks positions of NASICON-type phase $Na_3Sc_2(PO_4)_3$ are indicated by the vertical line. Y_{obs}: experimental intensity, Y_{cal}: calculated intensity.

3.3. Microstructural analysis

Fig. 4 shows SEM micrographs of the fracture surfaces for $Na_{3.4}Al_xSc_{2-x}Si_{0.4}P_{2.6}O_{12}$ ($1.0 \leq x \leq 1.7$) glass-ceramics crystallized at T_x for 3 h, as well as the micrograph of the $x = 1.7$ glass-ceramic obtained at T_x for 6 h. All samples exhibit dense microstructures, which confirms that the glass-ceramic route obtains NASICON materials with low porosity [15]. This result is expected when the densities of the glass and the crystalline phase are similar, which reduces the contraction stresses responsible for porosity during the transformation of glass to glass-ceramic [32].

On the other hand, it is also noted that the increase of aluminum promotes a decrease in grain size. Thus, the largest grain size is exhibited for the $x = 1.0$ glass-ceramic. We attribute this result to the presence of NASICON crystals before the heat treatment (as discussed in Section 3.2) in the precursor sample, i.e., the grains already formed grow even more with the heat treatment at T_x for 3 h. Besides, due to their high stability against crystallization, samples with higher aluminum content probably present slower crystallization kinetics and, thus, small grains are formed. As seen by thermal analysis (Section 3.1), the addition of aluminum also favors the thermal stability of glasses against crystallization.

Regarding the glass-ceramics with $x = 1.7$, the presence of smooth surfaces on micrographs (typical appearance of glassy phase) clearly shows that the heat treatment performed at T_x for 3 h and 6 h did not allow the total crystallization of parent glass. This result is in good agreement with that obtained by DSC (Section 3.1) and X-ray (Section 3.2) analyses.

3.4. Ionic conductivity

Fig. 5a illustrates the complex impedance spectra at 150 °C for the glass-ceramics with $x = 1.0$ and 1.5 obtained by heat treatment at T_x for 3 h and of the devitrified sample ($x = 0.0$). The formation of a single semi-circle is observed in all impedance plots, thus representing the sum of the electrical responses of the grain and grain boundary, i.e., the total electrical response of the sample. The ionic character of the electrical conductivity is confirmed by the straight line formed at lower frequencies in Fig. 5a. As known, this behavior results from blocking Na^+ ions in the electrode-sample interface.

On the other hand, as the impedance data values were corrected by the geometric parameter of each sample (l/A, l is the sample's thickness and A its surface area), the intercept of the semi-circles with the x-axis at lower frequencies indicates the total resistivity (ρ_{Total}). Thus, an increase in electrical resistivity as the Al^{3+} content increases from $x = 0.0$ to 1.5 is noted in Fig. 5a.

The total ionic conductivities (σ_{Total}) of glass-ceramics were calculated from the inverse of total resistivity ($\sigma_{Total} = 1/\rho_{Total}$) in the

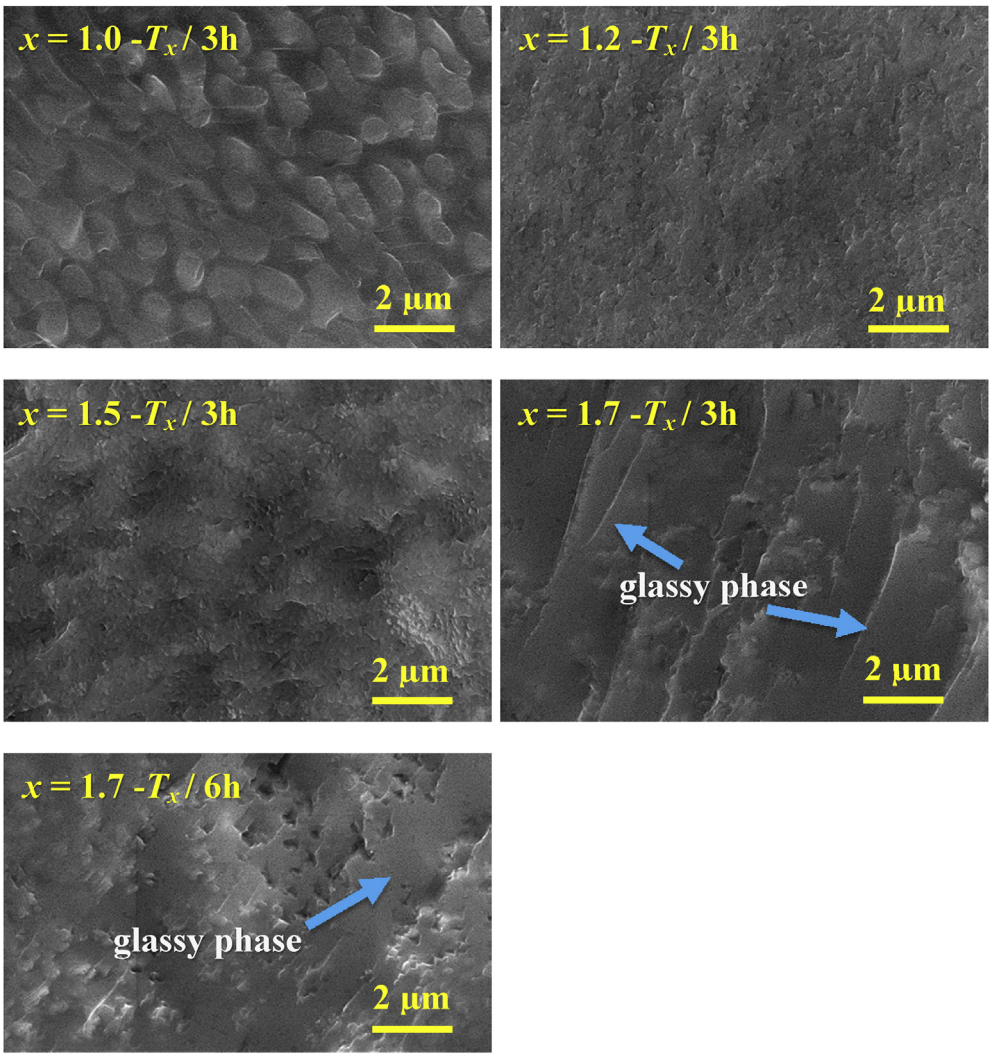

Fig. 4. SEM micrographs of the fracture surface of $Na_{3.4}Al_xSc_{2-x}Si_{0.4}P_{2.6}O_{12}$ ($1.0 \leq x \leq 1.7$) glass-ceramics obtained after crystallization of the precursor glass at T_x for 3 h, and also at T_x for 6 h for the sample with $x = 1.7$.

50 °C – 200 °C temperature range. Fig. 5b shows the evolution of σ_{Total} as a function of the inverse of temperature.

The linear regression of the experimental data of Fig. 5b was performed assuming an Arrhenius-like behavior:

$$\sigma_{Total} = \sigma_o \exp(-E_a / k_B T) \quad (2)$$

where σ_0 is the pre-exponential factor, E_a the activation energy for total conductivity, and k_B and T have their usual meanings.

The pre-exponential term of the Arrhenius equation depends on the concentration of charge carriers (n), the attempt frequency (ν_0), the ionic charge (Ze, where Z is the ion valence and e the electron charge), and the jump distance (λ) [22]:

$$\sigma_0 \approx n(Ze)^2 \lambda^2 \nu_0 / k_B T \quad (3)$$

As can be noted from Eq. (3), an estimation of the expected value of the pre-exponential parameter can be performed if the values of n, λ, and ν_0 are known. Thus, we have carried out a determination of the carrier concentration and the attempt frequency using Eq. (4) and Eq. (5) [33–35], respectively. Note that in Eq. (5), we have assumed that $\lambda \sim (1/n)^{1/3}$ [36] to calculate the ν_0 frequency parameter.

$$n = 3.4(\rho_{bc} N_A / F_w) \quad (4)$$

$$\nu_0 = (1/\lambda)\left(\sqrt{2E_a / M_{Na^+}}\right) \quad (5)$$

where ρ_{bc} is the bulk crystal density (calculated from Eq. (1), see Table 2), N_A the Avogadro's number, F_w the formula weight, M_{Na}^{+} the mass of the sodium ion, and E_a the activation energy for ionic conduction.

We have taken 373 K as a reference temperature in Eq. (3) considering that the variations of σ_0 are small in the temperature range used for impedance measurements in this work (50 – 300 °C).

Table 3 summarizes the logarithm of the pre-exponential factor ($\log \sigma_0$), the total activation energy (E_a), and the total ionic conductivity (σ_{Total}) obtained from the linear regression of the experimental data in Fig. 5b. The logarithm of the pre-exponential term ($\log \sigma_{0\text{-es}}$) estimated from Eq. (3) is also listed, as well as the jump distances (λ), the calculated (Eq. (5)) attempt frequencies (ν_0), and the carrier concentrations (n) (Eq. (4)).

Note the good agreement between the experimental value of the logarithm of the pre-exponential term ($\log \sigma_0$) with that

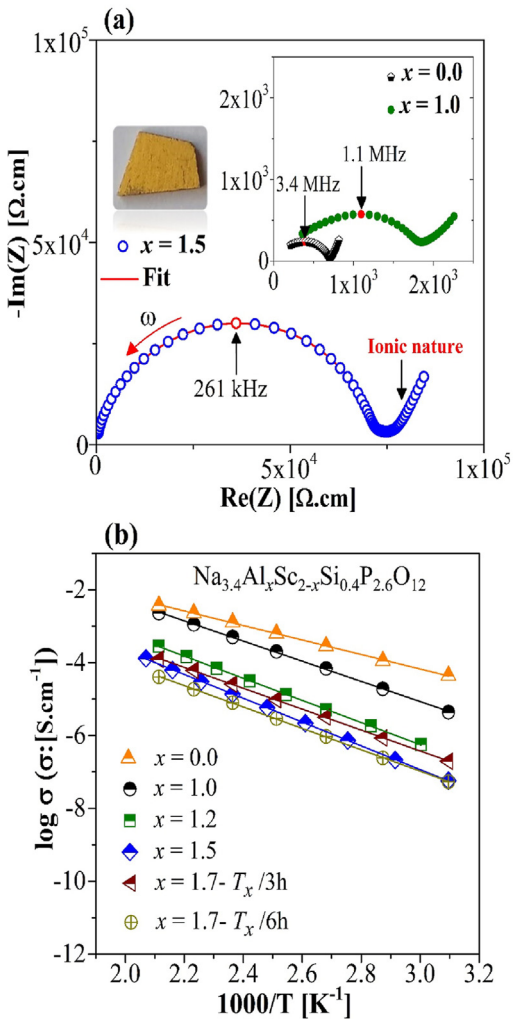

Fig. 5. (a) Complex impedance spectra at 150 °C of the devitrified sample ($x = 0.0$) and for $Na_{3.4}Al_xSc_{2-x}Si_{0.4}P_{2.6}O_{12}$ (x = 1.0, 1.5) glass-ceramics. Photo-image of the x = 1.5 gold-sputtered sample. (b) Arrhenius plot of the devitrified sample ($x = 0.0$) and for $Na_{3.4}Al_xSc_{2-x}Si_{0.4}P_{2.6}O_{12}$ ($1.0 \leq x \leq 1.7$) glass-ceramics obtained by heat treatment at T_x for 3 h, and also at T_x for 6 h for sample with $x = 1.7$. Solid lines in (b) represent the linear fitting of the experimental data, which resulted in correlation coefficients higher than 0.999.

estimated from Eq. (3) ($\log \sigma_{0\text{-es}}$), which are close to 2.0 as predicted for ionic conductors [36,37]. As also seen in Table 3, both σ_0 values in samples containing aluminum do not change with the increase of x. As previously mentioned, this result is expected since the Al^{3+}/Sc^{3+} isovalent substitution performed in the $Na_{3.4}Al_xSc_{2-x}Si_{0.4}P_{2.6}O_{12}$ series does not promote the addition of extra Na^+ ions, and the number of charge carrier per unit formula is constant. Thus, since σ_0 does not vary significantly, the changes in total ionic conductivity of $Na_{3.4}Al_xSc_{2-x}Si_{0.4}P_{2.6}O_{12}$ glass-ceramics are only attributed to the variation of activation energy, according to Eq. (2).

Although the presence of $Na_3Al_2(PO_4)_3$ undesired phase and also a remaining glassy phase, as shown by X-ray result (Fig. 2b), glass-ceramics with $x = 1.7$ show higher or similar conductivities than $x = 1.5$ sample (see Table 3 and Fig. 5b). Since $Na_3Al_2(PO_4)_3$ presents poor ionic conductivity [38], this increase in ionic conductivity should be attributed to a conductive glassy phase. This phenomenon, i.e., the increase of ionic conductivity by a conductive glassy phase, has already been suggested in the case of $Na_{1+x}Al_xGe_{2-x}(PO_4)_3$ (NAGP) glass-ceramics [39]. Composition with $x = 0.0$ (devitrified sample) presents slightly higher activation energy than the ceramic synthesized by Guin et al. (0.337 eV) [6]. This result is explained by the uncontrolled crystallization of our aluminum-free sample, which affects its microstructure and electrical properties.

Fig. 6 illustrates the variation of the total ionic conductivity at 25 °C, of the activation energy, and unit-cell volume of NASICON structure as a function of aluminum content (x). It is noted that the activation energy increases as the volume of the NASICON cell decrease from $x = 0.0$ to 1.5. This result can be understood since the contraction of unit cell volume causes a reduction in the bottleneck size through which charge carriers (Na^+) migrate within the material [3]. In other words, the ions migrate with greater difficulty through the narrow bottlenecks in samples with higher aluminum content, and this is reflected in the highest values of activation

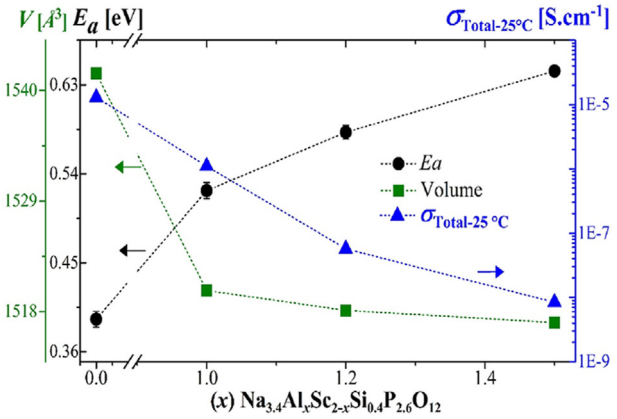

Fig. 6. Total ionic conductivity at 25 °C ($\sigma_{\text{Total-25°C}}$), activation energy for total ionic conductivity (E_a) and the unit cell volume (V) of NASICON structure as a function of Al^{3+} content (x) in $Na_{3.4}Al_xSc_{2-x}Si_{0.4}P_{2.6}O_{12}$ ($0.0 \leq x \leq 1.5$) compounds. Dashed lines serve as a guide for the eye. In most cases, error bars are smaller than the size of the symbols. Results of $x = 1.7$ composition are not included since NASICON is not a single-phase in these glass-ceramics.

Table 3
Total ionic conductivity at 25 °C ($\sigma_{\text{Total-25°C}}$) and 200 °C ($\sigma_{\text{Total-200°C}}$), activation energy ($E_a$), the logarithm of the pre-exponential factor ($\log \sigma_0$) determined from the linear regression of the Arrhenius plot (Fig. 5b) and Eq. (3) ($\log \sigma_{0\text{-es}}$), jump distances ($\lambda$), the attempt frequencies (ν_0), and carrier concentrations (n) for $Na_{3.4}Al_xSc_{2-x}Si_{0.4}P_{2.6}O_{12}$ glass-ceramics. The number within parentheses indicates the mathematical error of the last digit.

sample	E_a	$\log \sigma_0$	$\sigma_{\text{Total-25°C}}$	$\sigma_{\text{Total-200°C}}$	λ	ν_0	n	$\log \sigma_{0\text{-es}}$
x	[eV]	σ_0: [S cm^{-1}]	[S cm^{-1}]	[S cm^{-1}]	[10^{-8} cm]	[10^{12} s^{-1}]	[10^{22} Na^+ cm^{-3}]	$\sigma_{0\text{-es}}$: [S cm^{-1}]
0.0	0.393 (8)	1.78 (2)	1.3×10^{-5} [a]	3.9×10^{-3}	4.22	4.30	1.33	2.70
1.0	0.523 (8)	2.88 (9)	1.1×10^{-6} [a]	2.0×10^{-3}	4.21	4.98	1.34	2.77
1.2	0.582 (7)	2.58 (8)	5.4×10^{-8} [a]	2.4×10^{-4}	4.21	5.25	1.34	2.79
1.5	0.644 (2)	2.81 (2)	8.1×10^{-9} [a]	8.8×10^{-5}[a]	4.21	5.52	1.34	2.81
1.7–3h	0.569 (4)	2.18 (5)	3.6×10^{-8} [a]	1.3×10^{-4}	–	–	–	–
1.7–6h	0.583 (5)	1.97 (7)	1.2×10^{-8} [a]	5.5×10^{-5}	–	–	–	–

[a] Extrapolated values from Eq. (2).

energy and the low ionic conductivity [40,41] exhibited by these samples. The increase of E_a promoted a decrease in total ionic conductivity (at 25 °C) of up to 4 orders of magnitude when compared to the sample with $x = 0.0$. This result reveals that for samples with a constant number of Na^+ ions per unit formula, isovalent substitutions of the ion localized in octahedral positions (ScO_6) of the NASICON-type structure, by an ion with a smaller ionic radius, reduces the ionic conductivity due mainly to the narrowing of the bottleneck. In this sense, we want to suggest that an intermediate oxide with a trivalent ion whose ionic radius is similar (or higher) to that of Sc^{3+}, should be added to favor the synthesis of the $Na_{3.4}Sc_2Si_{0.4}P_{2.6}O_{12}$ compound by the glass-ceramic route.

4. Conclusions

Sodium ion-conducting NASICON glass-ceramics of $Na_{3.4}Al_xSc_{2-x}Si_{0.4}P_{2.6}O_{12}$ ($1.0 \leq x \leq 1.7$) composition are synthesized for the first time. The increase in the $T_x - T_g$ parameter as the x increases shows that the addition of Al_2O_3 oxide favors the glass-forming ability of precursor glasses. Low intensity or the absence of crystallization peak in samples with high aluminum content also indicates that Al_2O_3 hinders the crystallization of the precursor glass. The X-ray patterns of precursor glasses also confirm this idea since the samples with a higher content of Al^{3+} were fully amorphous. Thus, we demonstrated that the Al^{3+}/Sc^{3+} substitution favors the synthesis of $Na_{3.4}Al_xSc_{2-x}Si_{0.4}P_{2.6}O_{12}$ compounds by the glass-ceramic route.

From the structural characterization of glass-ceramics, it can be concluded that the Al^{3+} ions replace the Sc^{3+} ions in the NASICON structure, which promotes the contraction of the unit cell volume inferring the narrowing of the bottleneck size. This contraction of the unit-cell volume increases the activation energy and also decreases the total ionic conductivity of samples. Thus, the substitution of Sc^{3+} ions in the $Na_3Sc_2(PO_4)_3$ NASICON-type structure by an ion of the same valence and smaller atomic radius reduces the ionic conductivity of the material, confirming the rationale that reducing the bottleneck size has a negative effect on ionic conductivity.

Credit author statement

JFOM and ACMR designed the study; JFOM and AMNM carried out the experiments and characterizations; AMNM and JFOM contributed to sample preparation; AMNM performed the Rietveld analysis; JFOM, AMNM and ACMR contributed to the interpretation of the results and worked on the manuscript; ACMR supervised the project; All authors provided critical feedback and helped shape the research, analysis and manuscript.

Declaration of competing interest

The authors declare that they have no known competing financial interests or personal relationships that could have appeared to influence the work reported in this paper.

Acknowledgments

This work was supported by the Center of Research, Technology and Education in Vitreous Materials (CeRTEV, Fundação de Amparo à Pesquisa do Estado de São Paulo, Process number 2013/07793, via the CEPID program), CNPq (Conselho Nacional de Desenvolvimento Científico e Tecnológico, under Process No. 168682/2017-6 for JFOM and Process No. 141220/2016-3 for AMNM). This study was financed in part by the Coordenação de Aperfeiçoamento de Pessoal de Nível Superior - Brasil (CAPES) - Finance Code 001.

References

[1] L.O. Hagman, P. Kierkegaard, The crystal structure of $NaMe_2(PO_4)_3$; Me = Ge, Ti, Zr, Acta Chem. Scand. 22 (1968) 1822–1832, https://doi.org/10.3891/acta.chem.scand.22-1822.
[2] J.B. Goodenough, H.Y.-P. Hong, J.A. Kafalas, Fast Na^+-ion transport in skeleton structures, Mater. Res. Bull. 11 (1976) 203–220, https://doi.org/10.1016/0025-5408(76)90077-5.
[3] M. Guin, F. Tietz, Survey of the transport properties of sodium superionic conductor materials for use in sodium batteries, J. Power Sources 273 (2015) 1056–1064, https://doi.org/10.1016/j.jpowsour.2014.09.137.
[4] C. Jiang, H. Li, C. Wang, Recent progress in solid-state electrolytes for alkali-ion batteries, Sci. Bull. 62 (2017) 1473–1490, https://doi.org/10.1016/j.scib.2017.10.011.
[5] Z. Jian, Y.-S. Hu, X. Ji, W. Chen, NASICON-structured materials for energy Storage, Adv. Mater. 29 (2017) 1601925, https://doi.org/10.1002/adma.201601925.
[6] M. Guin, F. Tietz, O. Guillon, New promising NASICON material as solid electrolyte for sodium-ion batteries: correlation between composition, crystal structure and ionic conductivity of $Na_{3+x}Sc_2Si_xP_{3-x}O_{12}$, Solid State Ionics 293 (2016) 18–26, https://doi.org/10.1016/j.ssi.2016.06.005.
[7] T. Zinkevich, A. Fiedler, M. Guin, F. Tietz, O. Guillon, H. Ehrenberg, S. Indris, Na+ ion mobility in $Na_{3+x}Sc_2(SiO_4)_x(PO_4)_{3-x}$ ($0.1 < x < 0.8$) observed by 23Na NMR spectroscopy, Solid State Ionics 348 (2020) 115277, https://doi.org/10.1016/j.ssi.2020.115277.
[8] J.M. Winand, A. Rulmont, P. Tarte, Ionic conductivity of the $Na_{1+x}M^{III}_xZr_{2-x}(PO_4)_3$ systems (M = Al, Ga, Cr, Fe, Sc, In, Y, Yb), J. Mater. Sci. 25 (1990) 4008–4013, https://doi.org/10.1007/BF00582473.
[9] H. Aono, E. Sugimoto, Ionic conductivity and Sinterability of NASICON-type ceramics: the systems $NaM_2(PO_4)_{3+y}Na_2o$ (M = Ge, Ti, Hf, and Zr), J. Am. Ceram. Soc. 79 (1996) 2786–2788, https://doi.org/10.1111/j.1151-2916.1996.tb09052.x.
[10] H. Park, K. Jung, M. Nezafati, C.S. Kim, B. Kang, Sodium ion diffusion in Nasicon ($Na_3Zr_2Si_2PO_{12}$) solid electrolytes: Effects of excess sodium, ACS Appl. Mater. Interfaces (2016), https://doi.org/10.1021/acsami.6b09992.
[11] T. Pareek, S. Dwivedi, B. Singh, D. Kumar, P. Kumar, S. Kumar, $LiSnZr(PO_4)_3$: NASICON-type solid electrolyte with excellent room temperature Li^+ conductivity, J. Alloys Compd. 777 (2019) 602–611, https://doi.org/10.1016/j.jallcom.2018.10.384.
[12] S.H. Santagneli, H.V.A. Baldacim, S.J.L. Ribeiro, S. Kundu, A.C.M. Rodrigues, C. Doerenkamp, H. Eckert, Preparation, structural characterization, and electrical conductivity of highly ion-conducting glasses and glass ceramics in the system $Li_{1+x}Al_xSn_yGe_{2-(x+y)}(PO_4)_3$, J. Phys. Chem. C 120 (2016) 14556–14567, https://doi.org/10.1021/acs.jpcc.6b04839.
[13] V.A. Vizgalov, T. Nestler, L.A. Trusov, I.A. Bobrikov, O.I. Ivankov, M.V. Avdeev, M. Motylenko, E. Brendler, A. Vyalikh, D.C. Meyer, D.M. Itkis, Enhancing lithium-ion conductivity in NASICON glass-ceramics by adding yttria, CrystEngComm 20 (2018) 1375–1382, https://doi.org/10.1039/c7ce01910f.
[14] G.S. Sundar, G. Suman, K.N. Kumar, D.P. Dutta, R.B. Rao, Investigation on the applicability of high Na-ion conducting $Na_{3+x}[Zr_xSc_{2-x}(PO_4)_3]$ glass-ceramic electrolyte for use in safer Na-ion batteries, J. Phys. Chem. Solid. 126 (2019) 209–218, https://doi.org/10.1016/j.jpcs.2018.11.016.
[15] J.F. Ortiz-Mosquera, A.M. Nieto-Muñoz, A.C.M. Rodrigues, New $Na_{1+x}Ge_2(SiO_4)_x(PO_4)_{3-x}$ NASICON series with improved grain and grain boundary conductivities, ACS Appl. Mater. Interfaces 12 (2020) 13914–13922, https://doi.org/10.1021/acsami.9b23065.
[16] A.M. Nieto-Muñoz, J.F. Ortiz-Mosquera, A.C.M. Rodrigues, Novel sodium superionic conductor of the $Na_{1+y}Ti_2Si_yP_{3-y}O_{12}$ series for application as solid electrolyte, Electrochim. Acta 319 (2019) 922–932, https://doi.org/10.1016/j.electacta.2019.07.032.
[17] T. Okura, K. Kawada, N. Yoshida, H. Monma, K. Yamashita, Synthesis and Na^+ conduction properties of Nasicon-type glass-ceramics in the system Na_2O–Y_2O_3–R_2O_3–P_2O_5–SiO_2 (R = rare earth) and effect of Y substitution, Solid State Ionics 262 (2014) 604–608, https://doi.org/10.1016/j.ssi.2013.10.043.
[18] A.M. Cruz, E.B. Ferreira, A.C.M. Rodrigues, Controlled crystallization and ionic conductivity of a nanostructured $LiAlGePO_4$ glass-ceramic, J. Non-Cryst. Solids 355 (2009) 2295–2301, https://doi.org/10.1016/j.jnoncrysol.2009.07.012.
[19] A.M. Nieto-Muñoz, J.F. Ortiz-Mosquera, A.C.M. Rodrigues, The impact of heat-treatment protocol on the grain size and ionic conductivity of NASICON glass-ceramics, J. Eur. Ceram. Soc. 40 (15) (2020) 5634–5645, https://doi.org/10.1016/j.jeurceramsoc.2020.05.026.
[20] J.F. Ortiz-Mosquera, A.M. Nieto-Muñoz, A.C.M. Rodrigues, Precursor glass stability, microstructure and ionic conductivity of glass-ceramics from the $Na_{1+x}Al_xGe_{2-x}(PO_4)_3$ NASICON series, J. Non-Cryst. Solids 513 (2019) 36–43, https://doi.org/10.1016/j.jnoncrysol.2019.03.008.
[21] G.D. Soraru, F. Babonneau, S. Maurina, J. Vicens, Sol-gel synthesis of SiBOC glasses, J. Non-Cryst. Solids 224 (1998) 173–183, https://doi.org/10.1016/S0022-3093(97)00463-8.
[22] A.M. Nieto-Muñoz, J.F. Ortiz-Mosquera, A.C.M. Rodrigues, The role of Al^{+3} on the microstructural and electrical properties of $Na_{1+x}Al_xTi_{2-x}(PO_4)_3$ NASICON glass-ceramics, J. Alloys Compd. 820 (2020) 153148, https://doi.org/10.1016/j.jallcom.2019.153148.
[23] E.M. Vogel, R.J. Cava, E. Rietman, Na^+ ion conductivity and crystallographic cell characterization in the Hf-NASICON system $Na_{1+x}Hf_2Si_xP_{3-x}O_{12}$, Solid State

Ionics 14 (1984) 1–6, https://doi.org/10.1016/0167-2738(84)90002-X.
[24] Oxford Cryosystems, Crystallographica Search-Match, J. Appl. Crystallogr. 32 (1999) 379–380, https://doi.org/10.1107/s0021889899004124.
[25] A.A. Coelho, J. Evans, I. Evans, A. Kern, S. Parsons, The TOPAS symbolic computation system, Powder Diffr. 26 (2011) S22–S25, https://doi.org/10.1154/1.3661087.
[26] A. Belskly, M. Hellendbrandt, V.L. Karen, P. Luksch, New developments in the inorganic crystal structure Database (ICSD): accessibility in support of materials research and design, Acta Crystallogr. Sect. B Struct. Sci. Cryst. Eng. Mater. B58 (2002) 364–369, https://doi.org/10.1107/S0108768102006948.
[27] J. Deubener, M. Allix, M.J. Davis, A. Duran, T. Höche, T. Honma, T. Komatsu, S. Krüger, I. Mitra, R. Müller, S. Nakane, M.J. Pascual, J.W.P. Schmelzer, E.D. Zanotto, S. Zhou, Updated definition of glass-ceramics, J. Non-Cryst. Solids 501 (2018) 3–10, https://doi.org/10.1016/j.jnoncrysol.2018.01.033.
[28] M.L.F. Nascimento, L.A. Souza, E.B. Ferreira, E.D. Zanotto, Can glass stability parameters infer glass forming ability? J. Non-Cryst. Solids 351 (2005) 3296–3308, https://doi.org/10.1016/j.jnoncrysol.2005.08.013.
[29] R.D. Shannon, Revised effective ionic radii and systematic studies of interatomic distances in halides and chalcogenides, Acta Crystallogr. Section A. A32 (1976) 751–767, https://doi.org/10.1107/S0567739476001551.
[30] E.R. Losilla, M.A.G. Aranda, S. Bruque, M.A. París, J. Sanz, A.R. West, Understanding Na mobility in NASICON materials: a Rietveld, ^{23}Na and ^{31}P MAS NMR, and impedance study, Chem. Mater. 10 (1998) 665–673, https://doi.org/10.1021/cm970648j.
[31] A.R. West, Solid State Chemistry and its Applications, John Wiley, United Kingdom, 2014, https://doi.org/10.1107/s0108768185002476.
[32] A. Watanabe, M. Mitsudou, S. Kihara, Y. Abe, Preparation of void-free calcium phosphate glass-ceramics, J. Am. Ceram. Soc. 72 (1989) 1499–1500, https://doi.org/10.1111/j.1151-2916.1989.tb07687.x.
[33] T. Krauskopf, C. Pompe, M.A. Kraft, W.G. Zeier, Influence of lattice dynamics on Na^+ transport in the solid electrolyte $Na_3PS_{4-x}Se_x$, Chem. Mater. 29 (2017) 8859–8869, https://doi.org/10.1021/acs.chemmater.7b03474.
[34] M.A. Kraft, S.P. Culver, M. Calderon, F. Böcher, T. Krauskopf, A. Senyshyn, C. Dietrich, A. Zevalkink, J. Janek, W.G. Zeier, Influence of lattice polarizability on the ionic conductivity in the lithium superionic argyrodites Li_6PS_5X (X = Cl, Br, I), J. Am. Chem. Soc. 139 (2017) 10909–10918, https://doi.org/10.1021/jacs.7b06327.
[35] M.J. Rice, W.L. Roth, Ionic transport in super ionic conductors: a theoretical model, J. Solid State Chem. 4 (1972) 294–310, https://doi.org/10.1016/0022-4596(72)90121-1.
[36] M.L.F. Nascimento, A.C. Martins Rodrigues, J.L. Souquet, Microscopic and thermodynamic interpretations of experimental data on ionic conductivity in lithium silicate glasses, Phys. Chem. Glas. - Eur. J. Glas. Sci. Technol. Part B. 51 (2010) 69–77.
[37] J.-L. Souquet, M.L.F. Nascimento, A.C.M. Rodrigues, Charge carrier concentration and mobility in alkali silicates, J. Chem. Phys. 132 (2010), 034704, https://doi.org/10.1063/1.3271154.
[38] L. Moreno-Real, P. Maldonado-Manso, L. Leon-Reina, E.R. Losilla, F.E. Mouahid, M. Zahir, J. Sanz, Glasses and crystalline $A_3Al_2(PO_4)_3$ (A = Na, Li): an impedance and ^{31}P, ^{27}Al, ^{23}Na and ^{7}Li MAS-NMR study, J. Mater. Chem. 12 (2002) 3681–3687, https://doi.org/10.1039/b206855a.
[39] J.F. Ortiz-Mosquera, A.M. Nieto-Muñoz, H. Bradtmüller, H. Eckert, A.C.M. Rodrigues, Isothermal evolution of phase composition, structural parameters, and ionic conductivity in $Na_{1+x}Al_xGe_{2-x}(PO_4)_3$ glass-ceramics, J. Non-Cryst. Solids 533 (2020) 119725, https://doi.org/10.1016/j.jnoncrysol.2019.119725.
[40] B.E. Taylor, A.D. English, T. Berzins, New solid ionic conductors, Mater. Res. Bull. 12 (1977) 171–181, https://doi.org/10.1016/0025-5408(77)90161-1.
[41] A. Martínez-Juárez, C. Pecharromán, J.E. Iglesias, J.M. Rojo, Relationship between activation energy and bottleneck size for Li^+ ion conduction in NASICON materials of composition $LiMM'(PO_4)_3$; M, M' = Ge, Ti, Sn, Hf, J. Phys. Chem. B 102 (1998) 372–375, https://doi.org/10.1021/jp973296c.